MASS MOVEMENT RECONSTRUCTION AND BOULDER SIZE-FREQUENCY DISTRIBUTION OF A 3.4 km-LONG MARTIAN LANDSLIDE LOCATED IN SIMUD VALLIS

M. Pajola[1], M. Mergili[2], P. Cambianica[1], A. Lucchetti[1], M.T. Brunetti[3], A. Guimpier[4], M. Mastropietro[5], G. Munaretto[1], S. Conway[4], J. Beccarelli[6], G. Cremonese[1]. [1]INAF-Astronomical Observatory of Padova, Vic. Osservatorio 5, 35122 Padova, Italy (maurizio.pajola@inaf.it); [2]University of Graz, Graz, Austria; [3]Research Institute for Geo-Hydrological Protection – Italian National Research Council, Perugia, Italy; [4]Laboratoire de Planétologie et Géosciences, UMR6112 CNRS, Nantes Université, Université d'Angers, Le Mans Université, France; [5]Braunschweig TU University, Braunschweig, Germany; [6]University of Padova, Padova, Italy.

Introduction: So far, mass movements have been observed on Earth, Mercury (e.g., [1]), Venus [2], the Moon [3], Phobos [4], asteroids [5], icy satellites [6] and comets [7]. Among terrestrial planets, Mars has been the most studied with respect to landslides (e.g., [8-12]). As on Earth, the morphology (e.g., area, volume, runout length, drop height, width and texture) of the landslide deposits on extra-terrestrial bodies depends on factors such as the slope of the topography, the collapse mechanism, the mechanical properties of the material, the presence of fluids and volatiles within the sliding material, and the local environmental conditions (e.g., gravitational acceleration). On the other hand, potential mass movement preparatory and triggering factors can vary from one planet to another. Indeed, on Earth the presence of a thick atmosphere means one of the main causes of landslides is rainfall, while for Mars the low-density atmosphere means this mechanism cannot be inferred for recent landslides. Since we have never directly observed any Martian landslide, their preparatory and triggering factors have to be inferred from their morphology and context.
In this work, we analyze a Martian landslide, focusing on the mass movement reconstruction and investigating its boulders size frequency distribution.

The Simud Vallis Landslide: The Simud Vallis landslide is a 3.4 km-long landslide (11°43'N - 322°54'E) that is located in Simud Vallis, a large outflow channel that together with Tiu Vallis once connected the Valles Marineris with the Chryse Planitia [13]. Multiple teardrop-shaped islands are present on Simud Vallis' floor, all elongated in the S–N direction of the flow [14] that incised the Mid-Noachian plateau [15]. The Simud Vallis landslide (hereafter called *SV landslide*) is located on the western side of one of such landforms (Fig. 1A, Fig. 1B). It is characterized by numerous boulders on its deposits. Recently, [16] studied the SV landslide to compare it with similarly sized terrestrial analogues. In particular, by using the HiRISE images [17] and through the use of the crater-size frequency distribution [18] technique, [16] estimated the maximum age of formation of this landslide to be ~4.5 ± 4 Ma, i.e. Late Amazonian period of Mars

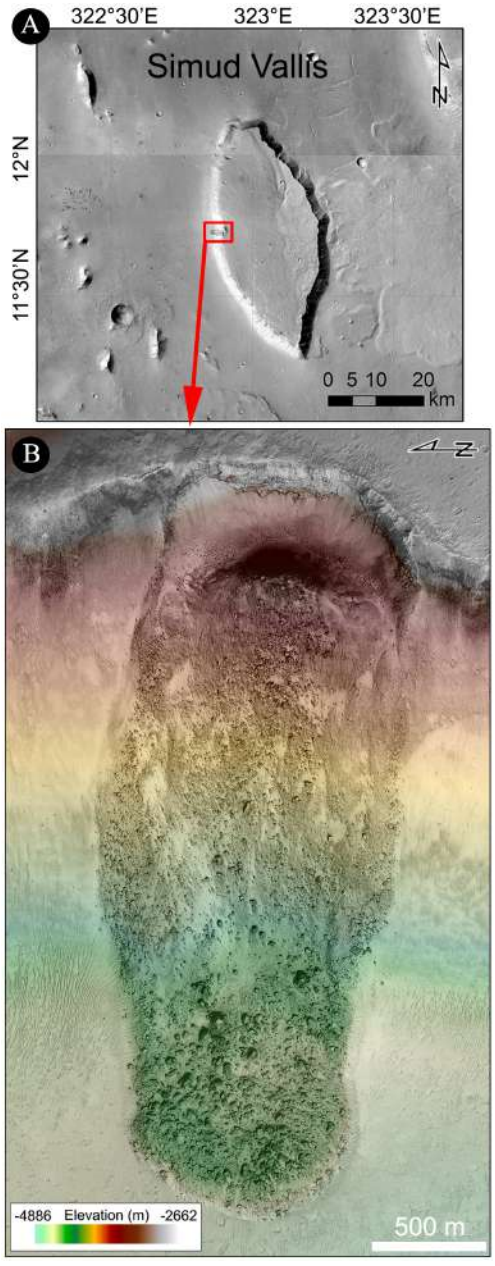

Fig. 1: A) The teardrop-shaped island where the SV landslide is located. B) The HiRISE image showing the SV landslide, together with the elevation values (in metres) derived from the HiRISE DTM overlaid in transparency.

geochronology. Afterwards, [16] modelled the SV landslide with the numerical simulation software *SHALTOP* [19], but the results only showed some moderate correspondence between the observed and the simulated flow areas and deposits, and the authors concluded that their results were not fully conclusive regarding the landslide mechanism.

Results and Discussion: Based on the visual criteria, the Simud Vallis landslide can be interpreted as a complex landslide involving both a rotational slide, hereafter called *stage 1*, and a flow, hereafter called *stage 2*. By using the 2 m-scale HiRISE DEM of [16] we have reconstructed the initial terrain surface, allowing us to estimate the release and deposition heights and volumes related to the two different stages of the landslide. For stage 1, we suggest a rotational slide with a total volume of 54.0 $\cdot 10^6$ m^3 [20]. Most of this initial volume was then involved in the stage 2 flow, whereas 13.4 $\cdot 10^6$ m^3 of it remained perched in the source area. The post-event DEM revealed a stage 2 deposition volume of 48.7 $\cdot 10^6$ m^3, indicating a volume increase of 20% with respect to the stage 2 release value, due to the generation of pore space during the flow. This confirms the overall plausibility of the reconstruction, even though the exact shape of the stage 1 deposition and the stage 2 release mass remain uncertain. The stage 2 flow has been numerically reconstructed with the *r.avaflow* software [21,22]. The general patterns of the flow, including the formation of a steep frontal scarp and lateral levees, is reproduced by the simulation [20]. However, the height of the modelled deposit is slightly overestimated in the frontal part, particularly since our model result does not include the assumed 20% pore space of the observed deposit. Moreover, when compared to the observed deposit, our simulation results show a very slight southward turn of the mass on the relatively flat deposition area. Our best-fit simulation suggests an extremely rapid stage 2 flow, which is suddenly released from the stage 1 deposit. This is supported by the fact that the landslide deposit exhibits a set of trenches that align parallel to the local direction of motion, indicative of a likely fast-moving flow mechanism for the emplacement of the failed materials. The simulated runout area based on *r.avaflow* clearly shows a higher degree of correspondence to the observed runout area of the SV landslide than the simulated runout area based on *SHALTOP* [16]. We attribute this improved model performance to a more appropriate definition of the release mass, as well as to the assumption of a viscous flow, which is most probably more realistic than the previous assumption of a purely frictional flow.

By using two 0.25 m-scale HiRISE images [17] we have manually identified and counted >130,000 boulders located along the landslide [20]. As predicted by landslide particle size segregation, the identified boulders are not homogenously distributed along the landslide. The highest spatial density of boulders is located at the front of the deposit, where the biggest boulders with sizes larger than 20 m are also present (Fig. 1B). The boulder density increases also inside the lateral levees of the landslide and where the remnants of the mass that detached during stage 1 are present. After deriving the boulder size-frequency distribution in the size range 1.75–59.2 m (the total number of boulders ≥1.75 m being 24,073), we have identified that the best fitting curve is the Weibull distribution [23], which results from sequential fragmentation and it is often used to describe the particle distribution derived from grinding experiments [24-26]. This suggests that while the SV landslide formed and was moving downslope, it broke-up the rocky constituents in a sequential way, rather than in a sudden, single-event fragmentation [20].

Acknowledgments: This work was supported by the Italian Space Agency (ASI-INAF agreement no. 2020-17-HH.0). SJC and AG are grateful for the support from CNES and the INSU Programme National de Planétologie.

References: [1] Xiao, Z. & Komatsu, G. 2013. PSS, 82, 62. [2] Malin, M. C., 1992. JGR, 97, 16337. [3] Brunetti, M. T. et al., 2015. Icarus, 260, 289. [4] Shi, X., J. et al., 2016. GRL, 43, 12371. [5] Massironi, M. et al., 2012. PSS, 66, 125. [6] Singer, K. N. et al., 2012. Nat.Geo. 5, 574. [7] Lucchetti, A. et al., 2019. GRL, 46, 14336. [8] Quantin, C., et al., 2004. PSS, 52, 1011. [9] Lucas, A. & Mangeney, A., 2007. GRL, 34, L10201. [10] Brunetti, M. T., et al., 2014. EPSL, 405, 156. [11] Crosta, G. B. et al., 2018. Earth Sp. Sci., 5(4), 89. [12] Sharp, R.P., 1973. JGR, 1896-1977 78, 4063. [13] Pajola, M. et al., 2016. Icarus, 268, 355. [14] Carr, M.H. & Clow, G.D., 1981. Icarus, 48 (1), 91. [15] Tanaka, K.L. et al., 2014. US Geological Survey. [16] Guimpier, A., et al., 2021. PSS, 206, 105303. [17] McEwen, A.S. et al., 2007. JGR, 112, E05S02. [18] Michael, G.G., & Neukum, G., 2010. EPSL, 294, 223. [19] Lucas, A. & Mangeney, A., 2007. GRL, 34, L10201. [20] Pajola, M. et al., 2022. Icarus, 375, 114850. [21] Mergili, M. & Pudasaini, S.P., 2021. https://www.avaflow.org. [22] Mergili, M., et al., 2017. Geo.M.D. 10, 553. [23] Weibull, W., 1951. J. Appl. Mech., 18, 837. [24] Grady, D.E. & Kipp, M.E., 1987. Ac. Pr., London, U.K, 429. [25] Brown, W.K. & Wohletz, K.H., 1995. J. Appl. Phys. 78, 2758. [26] Turcotte, D.L., 1997. Camb. Univ. Pr., Cambridge.